

## SIMULATIONS OF THIXOTROPIC LIQUIDS

Jos DERKSEN

Department of Chemical & Materials Engineering, University of Alberta, Edmonton AB, CANADA, T6G 2V4

### ABSTRACT

In thixotropic liquids the rheological properties depend on the liquid's deformation history. Clay suspensions (as encountered in oil sands mining) are a prominent example. Activated clay particles form a network. As a consequence of (ionic) transport limitations, the network is not an instantaneous feature; it takes time to build up, and also to break down, the latter as a result of deformation in the liquid. In this paper a procedure for detailed simulations of flow of viscous thixotropic liquids is outlined. The local viscosity of the liquid relates to the level of integrity of the network. The time-dependence of the liquid's rheology is due to the finite rate with which the network in the liquid builds up or breaks down. This concept has been incorporated in a lattice-Boltzmann discretization of the flow equations. With this methodology we study (at the macro-scale) the way thixotropic liquids are mobilized in mixing tanks, and we study (at the meso-scale) the drag force experienced by dense assemblies of coarse particles (e.g. sand) in thixotropic liquids.

### NOMENCLATURE

$d$	sphere diameter
$d_{ij}$	rate of strain tensor
$D$	impeller diameter
$f_0$	body force
$F_D, F_D^*, F_D^{**}, F_D^{***}$	(normalized) drag force
$H$	distance
$k_1, k_2$	thixotropy parameters
$N$	impeller speed
$u_i$	velocity component
$u_s$	superficial velocity
$t$	time
$T$	tank diameter
$x, y, z, r$	spatial coordinates
$\alpha + 1$	viscosity ratio
$\delta$	interparticle spacing
$\Delta$	lattice spacing
$\phi, \phi_{rcp}$	(random-close packing) solids volume fraction
$\dot{\gamma}, \dot{\gamma}_c$	(characteristic) deformation rate
$\lambda$	network parameter
$\mu_a, \mu_\infty, \mu_{ss}$	apparent, infinite-shear, steady-state viscosity
$\rho$	density
$\tau$	stress
Db	Deborah number
Re	Reynolds number
S	shear rate number

### INTRODUCTION

Many processing and mixing applications involve complex liquids. Examples are specifically abundant in food, pharmaceutical, and related industries; paper and pulp; polymer processing; and also oil sands mining and operations; the latter being the major motivation of the present work. One of the many intriguing phenomena that can occur in complex liquids is the development of a yield stress. Usually the yield stress is the consequence of a network being generated as a result of particle-particle or (macro-) molecular interactions of agents dispersed in a carrier phase. For example, in oil sands processing (Masliyah et al. 2004) clay particles get surface activated by (hot) water injection which initiates long range interactions between them. As a result of (ionic) transport limitations, the network is not an instantaneous feature; it takes time to build up, and also to break down as a result of deformations in the liquid. In non-homogeneous flows such time-dependent rheology (usually termed thixotropy) is closely linked to the flow dynamics as the (also non-homogeneous) level of network integrity is transported with the flow. It is expected that, from a fluid dynamics point of view, interesting situations occur when the time scales related to the network interfere with characteristic flow time scales.

In the applications that motivate the present work, geometrical complexity of the flows is an essential feature. On the macro scale one could think of flows in agitated vessels, or separation devices such as hydrocyclones. In many cases such process equipment operates in turbulent or (as is often the case with relatively viscous non-Newtonian liquids) transitional flow regimes. Also on the meso scale geometrical complexity matters: e.g. dense liquid-solid suspensions with complex interstitial liquid domains and moving solid particles. In any case: realistic numerical simulations of such flows requires flexibility in setting up computational grids, and above all computational efficiency in order to be able to resolve the flow including its flow structures to a sufficient level of detail. Previous studies (Derksen & Van den Akker 1999; Hartmann et al. 2004) have shown that the lattice-Boltzmann method (Succi 2001) is a versatile procedure for performing highly resolved computational fluid dynamics of Newtonian fluids. In this paper lattice-Boltzmann simulations of flows of thixotropic liquids in complexly shaped confinements at meso and macro scale are discussed.

A troubling issue regarding simulating non-Newtonian rheology is the steep increase of the number of parameters with increasing complexity of the model characterizing the liquid, and the need to (experimentally and/or computationally) determine their values. For this reason

we choose to limit the number of parameters by adopting a relatively simple thixotropy model.

### THIXOTROPY MODEL

The thixotropy model we have adopted is based on early work due to Storey & Merrill (1958), and Moore (1959), more recently reviewed and applied by Mujumdar et al. (2002). In this purely viscous (i.e. non-elastic) model we keep track of a scalar  $\lambda$  that varies between 0 and 1 and indicates the integrity of the network ( $\lambda=0$ : no network;  $\lambda=1$ : fully developed network). Its transport equation reads

$$\frac{\partial \lambda}{\partial t} + u_i \frac{\partial \lambda}{\partial x_i} = -k_1 \dot{\gamma} \lambda + k_2 (1 - \lambda) \quad (1)$$

(summation over repeated indices) with  $u_i$  the  $i$ th component of the fluid velocity vector, and  $\dot{\gamma} = \sqrt{2d_{ij}d_{ij}}$

a generalized deformation rate;  $d_{ij} = \frac{1}{2} \left( \frac{\partial u_j}{\partial x_i} + \frac{\partial u_i}{\partial x_j} \right)$  is the

rate of strain tensor. The first term on the right hand side of Eq. 1 indicates breakdown of the network due to liquid deformation; the second term is responsible for build-up of the network with a time constant  $k_2^{-1}$  associated to it. In the model, the apparent viscosity  $\mu_a$  is linked to the network integrity according to

$$\mu_a = \mu_\infty (1 + \alpha \lambda) \quad (2)$$

In a homogeneous shear field with shear rate  $\dot{\gamma}$ , the steady-state viscosity is

$$\mu_{ss} = \mu_\infty \left( 1 + \alpha \frac{k_2}{k_1 \dot{\gamma} + k_2} \right) \quad (3)$$

The parameter  $\mu_\infty$  can thus be interpreted as the infinite shear viscosity. The zero-shear viscosity is  $\mu_0 = \mu_\infty (1 + \alpha)$ . A typical representation of the steady-state rheology (Eq. 3) is given in Figure 1. The thixotropic liquid as defined by Eqs. 1 and 2 has four parameters:  $\mu_\infty, \alpha, k_1, k_2$ .

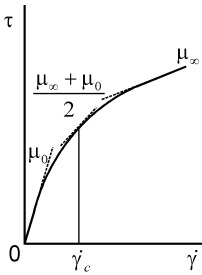


**Figure 1:** Steady-state rheology (Eq. 3) with  $\dot{\gamma}_c \equiv \frac{k_2}{k_1}$ .

### FLOW SOLVER AND SCALAR TRANSPORT MODELING

The lattice-Boltzmann method (LBM) is a well-established way to numerically solve the incompressible Navier-Stokes equations. The method originates from the lattice-gas automaton concept as conceived by Frisch, Hasslacher, and Pomeau in 1986. Lattice gases and lattice-Boltzmann fluids can be viewed as fictitious particles

moving over a regular lattice, and interacting with one another at lattice sites. These interactions (collisions) give rise to viscous behavior of the fluid, just as colliding/interacting molecules do in real fluids. Since 1987 particle-based methods for mimicking fluid flow have evolved strongly, as can be witnessed from review articles and text books (Chen & Doolen 1998; Succi 2001; Sukop & Thorne 2006).

The main reasons for employing the LBM for fluid flow simulations are its computational efficiency and its inherent parallelism, both not being hampered by geometrical complexity. More recently LBM has been applied to non-Newtonian fluid mechanics (Yoshino et al. 2007; Vikhansky 2008).

In this paper the LBM formulation of Somers (1993) has been employed which falls in the category of three-dimensional, 18 speed (D3Q18) models. Its grid is uniform and cubic. Planar, no-slip walls naturally follow when applying the bounce-back condition. For non-planar and/or moving walls (that we have in case we are simulating the flow in a mixing tank with a revolving impeller) an adaptive force field technique (a.k.a. immersed boundary method) has been used (Goldstein et al. 1993; Derksen & Van den Akker 1999). We have employed and validated this method extensively in previous studies involving (turbulent) flow in process equipment (e.g. Derksen & Van den Akker 2000; Derksen 2005).

For incorporating thixotropy, the viscosity needs to be made dependent on the local value of the network parameter  $\lambda$  (Eq. 2), and (more importantly) the transport equation for the network parameter (Eq. 1) needs to be solved. Solving scalar transport equations in a LBM context is an option (see e.g. Eggels & Somers 1995). It is, however, a relatively expensive approach in terms of computer memory usage: in order to solve for a single scalar we need to allocate as much memory as for solving the Navier-Stokes equations (i.e. 18 real values per lattice node in an 18 speed LBM).

Instead we solve Eq. 1 with an explicit finite volume discretization on the same (uniform and cubic) grid as the LBM. This way only two real values per lattice node need to be stored. An additional advantage of employing a finite volume formulation is the availability of methods for suppressing numerical diffusion. This is particularly important in the present application since Eq. 1 does not have a molecular or turbulent diffusion term; in order to correctly solve Eq. 1 we cannot afford to have significant numerical diffusion. As in previous works (Hartmann et al. 2006; Derksen 2008), TVD discretization with the Superbee flux limiter for the convective fluxes (Sweby 1994) was employed. We step in time according to an Euler explicit scheme.

### A BENCHMARK: PLANE POISEUILLE FLOW

Consider the flow between two fixed parallel plates at mutual distance  $H$  driven by a body force (force per unit volume)  $f_0$  in the wall-parallel direction (see Figure 2 for a definition of the flow and its coordinate system). The body force results in a linear shear stress profile in the liquid:  $\tau_{xz} = -f_0 z$ . In zero-inertia flow this directly

translates in a shear rate  $\dot{\gamma} = \left| \frac{-f_0 z}{\mu_a(z,t)} \right|$ . Given Eq. 2, and

since the system is homogeneous in  $x$ -direction the transport equation in the network parameter (Eq. 2) can be written as

$$\frac{\partial \lambda}{\partial t} = -k_1 \lambda \frac{f_0 |z|}{\mu_\infty (1 + \alpha \lambda)} + k_2 (1 - \lambda) \quad (4)$$

In the center of the channel ( $z=0$ ), Eq. 4 implies that  $\lambda$  depends on time according to an exponential function with time constant  $k_2^{-1}$ . In order to compare the implications of Eq. 4 for the way the network parameter and the velocity field depend on space ( $z$ ) and time, it was integrated numerically (with a fourth-order Runge-Kutta scheme) for  $z$  in the range  $-\frac{H}{2} < z < \frac{H}{2}$ . This provides us with a

representation of  $\lambda(z,t)$  that subsequently is used to determine  $\mu_a(z,t)$  (with help of Eq. 2) and integrate the velocity profile from the notion that  $\frac{\partial u_x}{\partial z} = -\frac{f_0 z}{\mu_a}$  with  $u_x = 0$  at  $z = \pm \frac{H}{2}$ . The results of this semi-analytical exercise can be directly compared with our numerical simulations.

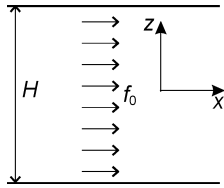


**Figure 2:** Plane Poiseuille flow definition.

In the simulations we start from a zero flow field of Newtonian liquid. Once that flow has fully developed (to a parabolic velocity profile in this case) the thixotropic rheology is switched on and we monitor the development of the network and associated apparent viscosity and velocity field. As the velocity scale we take the centerline velocity of the Newtonian liquid:  $u_0 = \frac{1}{8} \frac{f_0}{\mu_\infty} H^2$ ; the

Reynolds number has been defined as  $Re = \frac{\rho u_0 H}{\mu_\infty}$ . The

results in Figure 3 show very good agreement of the simulations and the semi-analytical solution. The time scales over which the flow switches from the Newtonian steady state to the non-Newtonian steady state, as well as the profiles of  $\lambda$  and  $u_x$  are well represented by the simulations. We see the development of the  $\lambda$ -profile in time: starting from zero  $\lambda$  increases quickest in the center of the channel where there is no deformation. Roughly at  $t = 50 \frac{H}{u_0} = \frac{2.5}{k_2}$  after switching on the thixotropic rheology the  $\lambda$  profile is close to steady. In the same time range the velocity profile has adapted itself to the new rheology; it has evolved from parabolic to more plug-flow like.

The assumption of zero-inertia as inferred to obtain the semi-analytical solution appears critical. In the right panel of Figure 3 we compare (at a single moment in time) the semi-analytical solution with simulation results at different Reynolds numbers. The trend is that the agreement clearly benefits from reducing the Reynolds number in the simulations. The results with  $Re < 1$  can hardly be distinguished and are close to the semi-analytical solution.

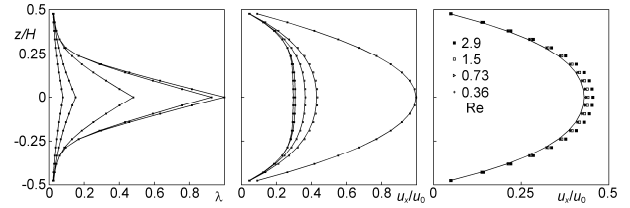


**Figure 3:** Left:  $\lambda$  profiles at various moments ( $tu_0/H = 1.6, 3.3, 13, 52,$  and  $210$ ;  $\lambda$  increases with time) after switching on thixotropic rheology. Middle: velocity profiles ( $tu_0/H = 0, 1.6, 3.3, 13,$  and  $52$ ; velocity decreases with time). Right: velocity profiles at  $tu_0/H = 1.6$  for four different Reynolds numbers. The left and middle panel have  $Re=0.73$ . Drawn curves: semi-analytical solutions; symbols: simulations.

## THIXOTROPIC LIQUIDS IN MIXING TANKS

We now turn to flows of thixotropic liquids in mixing tanks. The geometry of the mixing tank and the impeller are given in Figure 4, along with a definition of the coordinate system. The impeller, a Rushton turbine, is a de-facto standard impeller in mixing research and therefore allows for comparison with a large body of numerical and experimental data regarding Newtonian and (to a lesser extent) non-Newtonian liquids. It consists of a round disk with six flat blades mounted on its perimeter. The tank has baffles at its perimeter that enhance mixing as they prevent the liquid from rotating largely as a solid body under the influence of the revolving impeller. In this standard configuration all tank and impeller dimensions can be derived from the tank diameter  $T$  (see Figure 4), e.g. the impeller diameter  $D=T/3$ .

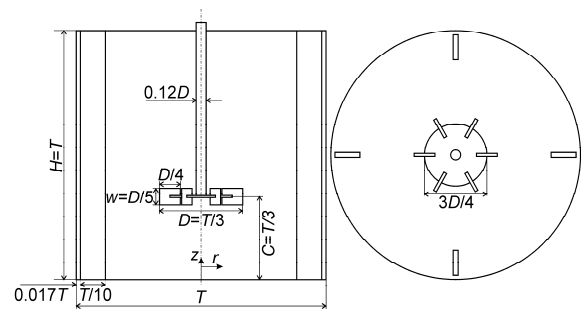


**Figure 4:** Stirred tank geometry and  $(r,z)$  coordinate system. Left: side view, right: top view.

In mixing of Newtonian liquids in stirred tanks the Reynolds number is traditionally defined as  $Re = \frac{\rho N D^2}{\mu}$  with  $N$  the impeller speed (in rev/s). In analogy we here

define the Reynolds number as  $Re = \frac{\rho ND^2}{\mu_\infty}$ . The

additional three dimensionless numbers if thixotropic liquid mixing is being considered are chosen as follows:

$Db = \frac{N}{k_2}$  the Deborah number (the ratio of liquid over

flow time scale),  $S = \frac{k_2}{k_1} \frac{1}{N} \equiv \frac{\dot{\gamma}_c}{N}$  the dimensionless shear

rate (inspection of Eq. 3 shows that  $\dot{\gamma}_c \equiv \frac{k_2}{k_1}$  is the shear at

which the liquid typically transits from infinite-shear to zero-shear behaviour, also see Fig. 1), and  $\alpha$  where  $\alpha + 1$  is a viscosity ratio.

The tanks to be simulated are of lab-scale size with a tank volume of typically 10 liter. A 10 liter tank with geometrical layout as given in Figure 4 has a diameter  $T=0.234$  m. The impeller diameter  $D=T/3=0.078$  m. With a liquid having  $\mu_\infty = 10^{-2}$  Pa·s and  $\rho=10^3$  kg/m<sup>3</sup> we generate mildly turbulent flow if the impeller spins with  $N=10$  rev/s:  $Re=6 \cdot 10^3$ . Commonly used thixotropic liquids have time constants in the range of 0.1 to 10 s (see e.g. Dullaert & Mewis 2005), so that the Deborah numbers fall in the range 1 to 100. To end up with laminar flow if the network would be fully developed ( $\lambda=1$  everywhere) we set  $\alpha + 1=100$ . To limit the parameter space, we set the shear rate number to the fixed value of  $S=1$  which represents the situation with the typical shear rate in the tank ( $N$ ) being the same as the liquid's characteristic shear rate  $\dot{\gamma}_c$ .

As mentioned above, the liquid flow dynamics was resolved using the lattice-Boltzmann method. In its basic implementation (as used in this study) the method applies a uniform, cubic grid. The spatial resolution of the grid was such that the tank diameter  $T$  equals 180 grid spacings  $\Delta$ . The time step is such that the impeller revolves once in 2000 time steps. The rotation of the impeller in the static grid is represented by an immersed boundary technique. As the default situation, the simulations were started from a zero liquid velocity field and a uniform network parameter  $\lambda=0$  (no network). Our primary interests are in how the flow develops towards a (quasi) steady state, what flow structures can be observed in (quasi) steady state, and what the influence of the Deborah number is on all this.

## Results

In Figure 5 we show the development of the tank-average structure parameter  $\langle \lambda \rangle$  after starting from a zero flow, and zero  $\lambda$  field. Clearly, the higher  $Db$  the slower the network develops. In addition, the path along which the three cases approach quasi steady state is very different. At  $Db=1$  the network builds up quicker than the flow that starts around the impeller can penetrate the bulk of the tank. This results in an initial overshoot of  $\langle \lambda \rangle$  with  $\lambda$  quickly increasing in the still quiescent parts of the tank. In a later stage the flow erodes the networked zones in the tank and decreases again after which a quasi steady state is reached. For  $Db=10$  the development towards steady-state has a relatively fast stage (with a time scale

associated to it of the order of  $k_2^{-1}$ ) and a slow stage taking of the order of 150 impeller revolutions. At the highest  $Db$  ( $Db=100$ ) the system very gradually goes towards steady state.

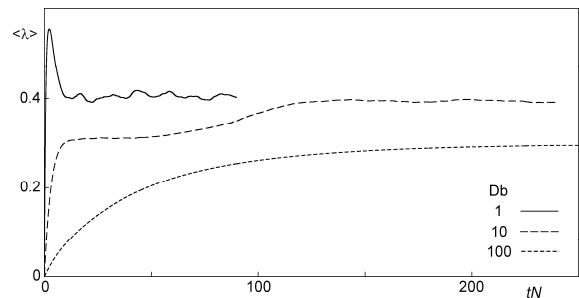


**Figure 5:** Time series of the tank-averaged  $\lambda$  for three values of  $Db$  when starting up from a zero flow, and zero  $\lambda$  field.

The  $Db=1$  case gives rise to a very inhomogeneous distribution of the apparent viscosity in the tank, with low levels close to the impeller and in the stream emerging from the impeller where the network is destroyed continuously due to liquid deformation, and high levels in the dead zones in (for instance) the upper corners (see Figure 6, upper center panel). This distribution creates active and relatively inactive regions in the tank. For comparison we also show in Figure 6 (upper left panel) a distribution of the apparent viscosity if  $Db=0$ , which we get if instead of a thixotropic liquid we have a time independent liquid with the steady-state rheology of Eq. 3. The apparent viscosity distributions with  $Db=1$  is very similar to the one with  $Db=0$  indicating that for  $Db=1$  (and the rest of the current conditions: flow geometry, other dimensionless numbers) the time dependence of the liquid is not strongly felt.

If  $Db=100$ , the liquid's time scales are much longer than almost all relevant flow time scales. In other words, the mixing is very fast compared to the build-up and breakdown of the network which leads to a fairly uniform (well-mixed) distribution of the apparent viscosity, see Figure 6 (upper right panel). This situation is comparable to a very slow chemical reaction taking place in a vigorously mixed tank. Under such conditions the tank can be considered ideally mixed with approximately uniformly distributed concentrations. At the specific settings of this simulation, the level of the apparent viscosity ultimately gets of the order of  $20\mu_\infty$  throughout the tank which corresponds to a Reynolds number of

$$Re_\alpha = \frac{\rho ND^2}{\mu_\alpha} \approx 300, \text{ indicating transitional flow.}$$

The most intriguing case is the one with  $Db=10$ . Some 40 revolutions after startup the system tends steady state. However, beyond 50 revolutions  $\langle \lambda \rangle$  starts slowly but systematically increasing again until it levels off after 150 revolutions after start-up. What happens in the slow part of the flow's development (between 50 and 150 revolutions) is a slow build-up of the network in the upper part of the tank which gradually pushes the impeller stream down until the liquids only recirculates underneath the impeller, see Figure 6 (lower three panels).

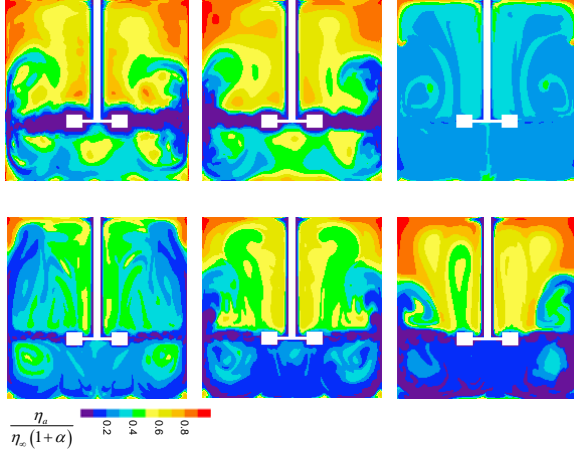


**Figure 6:** Snapshots of the apparent viscosity in a vertical cross section through the tank. Top row from left to right:  $Db=0$  at  $tN=60$ ,  $Db=1$  at  $tN=60$ ,  $Db=100$  at  $tN=250$ . Bottom row:  $Db=10$  and (from left to right)  $tN=50$ , 100, 210.

### SUSPENSIONS INVOLVING THIXOTROPIC LIQUIDS

Dense solid-liquid suspensions involving non-Newtonian carrier fluids are of practical relevance in applications such as oil sands mining, drilling of oil and gas wells, and food and pharmaceutical processing. Fundamental insights in the interactions of solid and liquid at the level of the solid particles could be relevant for a better understanding of the processes underlying these applications, and thus could help in process design and optimization. Also, process modeling (partly) based on computational fluid dynamics (CFD) at the macro-scale has become a viable and widely used approach. Multiphase CFD, however, requires closure relations for meso-scale phenomena such as the hydrodynamic interaction between the phases involved (Li & Kuipers 2003). A lot of research effort has been invested in developing and assessing closures for multiphase systems with a Newtonian carrier phase, such as drag force relations for random particle assemblies (Kandhai et al. 2003; Van der Hoef et al. 2005), and models for turbulent and granular fluctuations. In situations where the carrier phase behaves as a non-Newtonian liquid, the meso-scale fluid mechanics (hydrodynamic interactions, dispersed phase behavior) potentially becomes more complicated. This may have significant implications for the applicability of closures (based on Newtonian fluid concepts) for the meso-scale phenomena of suspensions with non-Newtonian liquids.

With the above in mind we have carried out computational research that aims at assessing non-Newtonian effects in dense solid-liquid suspensions, with a focus on the drag force and the way it depends on liquid properties and the solids volume fraction. The study is limited to suspensions consisting of monodisperse spheres with diameter  $d$  in a purely viscous thixotropic carrier liquid described by Eqs. 1 & 2. The sphere assemblies with solids volume fraction  $\phi$  are random and homogeneous; there are no large-scale (solids volume fraction) gradients. The liquid is forced through the spheres with a superficial velocity  $u_s$  such that the flow is slow, i.e. dominated by viscous forces rather than inertia. The computations measure the drag

force on the spheres. The average drag force on a sphere  $F_D$  is normalized with the Stokes drag on a sphere in a Newtonian liquid with viscosity  $\mu_\infty$ :  $F_D^* \equiv \frac{F_D}{3\pi\mu_\infty d u_s}$ .

The flow of thixotropic liquids through monosized sphere assemblies can be pinned down with a set of five dimensionless numbers. In this paper these have been chosen as  $Re_\infty = \frac{\rho u_s d}{\eta_\infty}$ ,  $Db = \frac{u_s}{dk_2}$ ,  $S = \frac{\dot{\gamma}_c d}{u_s}$ ,  $\alpha$ , and  $\phi$ .

This five-dimensional parameter space we limit by only considering a single, low value of  $Re_\infty = 0.06$ . We also fix the viscosity ratio to  $\alpha + 1 = 16$ . Since  $\alpha > 0$  the low value of the Reynolds number implies creeping flow conditions at all times.

The resolution of the simulations is such that the sphere diameter  $d$  is equal to 24 grid spacings. The diameter  $d$  is the so-called hydrodynamic diameter of the spheres. A calibration procedure (Ladd 1994) is used to relate the hydrodynamic diameter to the diameter in the lattice. This calibration depends on the viscosity, it has been carried out for  $\mu = \mu_\infty \left(1 + \frac{1}{2}\alpha\right)$ .

### Results for shear-thinning time independent liquids

Time-independent liquids have  $k_2 \rightarrow \infty$  so that  $Db=0$ . The two degrees of freedom left are the solids volume fraction  $\phi$  and  $S = \frac{\dot{\gamma}_c d}{u_s}$ .

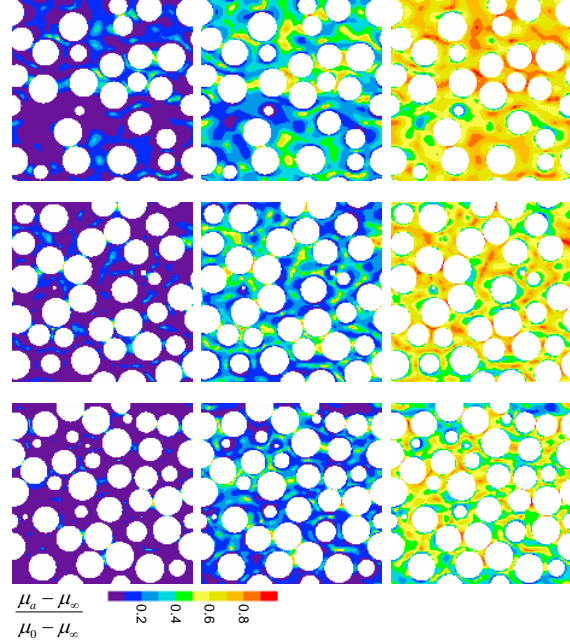


**Figure 7:**  $xz$ -cross sections through the flow domains, with the horizontal ( $x$ ) direction the direction of the mean flow. Shear-thinning, time-independent liquids. Colors indicate the apparent viscosity. From top to bottom  $\phi = 0.373$ , 0.459, and 0.530. From left to right  $S = 1$ , 4, and 16 respectively.

In Figure 7 we show contour plots of the distribution of the apparent viscosity in a cross section through the suspension after steady state has been reached. The cross

sections span the  $xz$ -plane of the cubic periodic domain with the  $x$ -direction the streamwise direction. The white circular disks are cross sections through the spherical particles. The higher  $S$ , the higher the apparent viscosity in the suspension gets. This is not surprising. At higher  $S$  (and thus higher  $\dot{\gamma}_c$ ) the transition from zero-shear viscosity to infinite-shear viscosity takes place at higher deformation rates (see Figure 1). Also the range of viscosities encountered in the suspension is a function of  $S$ : if the characteristic shear rate  $\dot{\gamma}_c$  of the liquid is of the same order as the shear rates encountered in the interstitial liquid, a relatively broad range of viscosities is anticipated.

The above observations are presented in a more quantitative sense in Figure 8. The figure shows (for two solids volume fractions) the doubly normalized drag force

$$F_D^{**} \equiv \frac{F_D^*}{F_{D^*}|_{S=0}},$$

the average apparent viscosity in the suspension, and (as a measure of the spread in viscosities in the liquid domain) the root-mean-square (rms) values of the deviations from the mean apparent viscosity. Interestingly  $\text{rms}(\mu_a)$  goes through a maximum with the location of the maximum dependent on the solids volume fraction: the higher  $\phi$  the further the maximum shifts to higher  $S$ . At higher  $\phi$  the space between the spheres gets narrower and (since the superficial velocity has a fixed value) the deformation rates in the liquid increase. As a result, the distribution of viscosities gets wider for higher  $S$ .

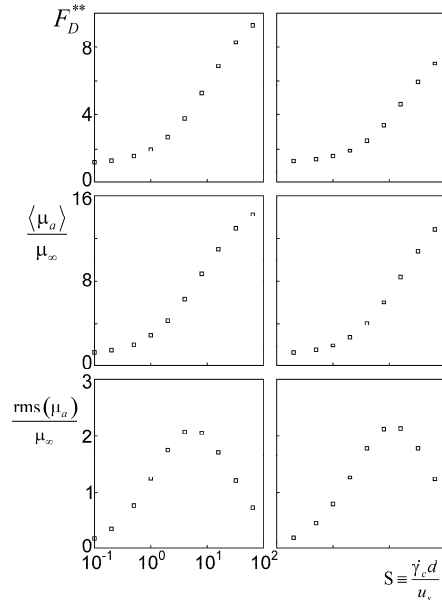


**Figure 8:** Doubly normalized drag force  $F_D^{**}$  (top); average apparent viscosity (middle); and root-mean-square values of the apparent viscosity as a function of  $S$  for two solids volume fractions: left:  $\phi=0.373$ ,  $\phi=0.530$ . Shear-thinning, time-independent liquids.

Eventually, the drag force is the result of an interplay between the liquid flow through the suspension and the resulting spatial viscosity distribution. The notion of the interaction between  $\dot{\gamma}_c$  and deformation rates in the

suspensions proofs helpful in scaling the doubly normalized drag force  $F_D^{**}$ . Critical regions in the suspension are the waists between nearby spheres. As a measure for the size of these waists we take

$$\delta \equiv d \left[ \left( \frac{\phi_{rcp}}{\phi} \right)^{1/3} - 1 \right]$$

with  $\phi_{rcp} = 0.62$  the solids volume fraction at random close packing. In Figure 9 we plot  $F_D^{**}$  as a function of  $\frac{\delta \dot{\gamma}_c}{u_s}$  for all cases with time-independent

rheology ( $Db=0$ ) considered. The drag force behaves fairly consistently over the wide range of solids volume fractions considered.

### Results for thixotropic liquids

Examples of steady-state viscosity distributions with thixotropic liquids are given in Figure 10. The most visible effect of thixotropy is a smearing-out of the viscosity fluctuations. This effect sets in beyond  $Db=0.2$  (the viscosity fields at  $Db=0$  and  $Db=0.2$  are almost the same). The smearing out is due to the time it takes to build up or break down the network. In an infinitely fast ( $Db=0$ ) liquid, locations where the network is formed or broken down coincide with places of respectively low (e.g. bigger voids in the suspension) and high (shear layers at solid surfaces) deformation rates. If the liquid needs time to respond to deformation conditions ( $Db>0$ ) the break-down and build-up processes are less localized with a smoother apparent viscosity field as the result.

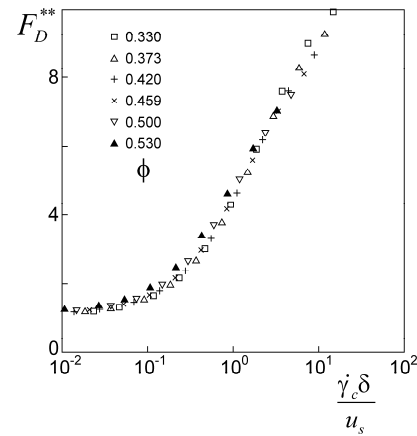


**Figure 9:** Doubly averaged drag force as a function of  $\frac{\delta \dot{\gamma}_c}{u_s}$  with  $\delta$  defined in the text. The different symbols relate to different solids volume fraction as indicated. Shear-thinning, time-independent liquids.

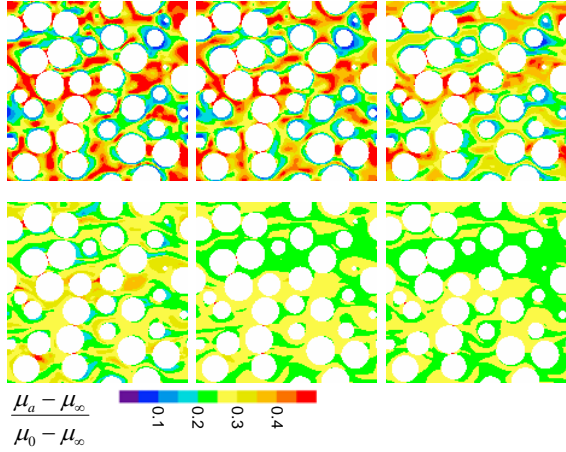


**Figure 10:**  $xz$ -cross sections through one flow domain, with the horizontal ( $x$ ) direction the direction of the mean flow.  $\phi=0.420$ ,  $S=4$ . Thixotropic simulations with (from left to right and top to bottom)  $Db=0, 0.2, 1.0, 5.0, 25.0, 125.0$ . Colors indicate the apparent viscosity.

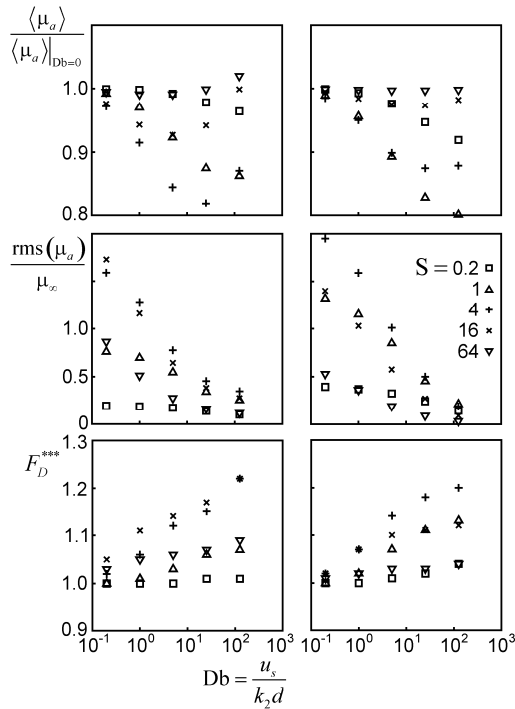


**Figure 11:** Sample simulation results with thixotropic liquids. From bottom to top: triply normalized drag force, rms of viscosity, and average viscosity as a function of  $Db$ . Left:  $\phi=0.530$ ; right:  $\phi=0.330$ . The different symbols denote different values of  $S$  as indicated.

In Figure 11 sample results of our thixotropic simulations are displayed, with  $Db$  as the independent variable. The triply normalized drag force is defined as  $F_D^{***} \equiv \frac{F_D^{**}}{F_D^{**}|_{Db=0}}$ .

In the way as displayed in Fig. 11, the behaviour is quite similar for different solids volume fractions, so that we only show the extremes of  $\phi$  as studied here. The effect of a smoother apparent viscosity field due to thixotropy is an increase in the drag force; in all cases considered  $F_D^{***} > 1$ . The effect of thixotropy on the drag force is not

very big; the maximum increase is approximately 20%, occurring for high  $Db$  in situations where the corresponding  $Db=0$  system had a large  $\text{rms}(\eta_a)$ .

## SUMMARY

In this paper we described simulations at the equipment (macro) scale and at the particle (meso) scale of the flow of thixotropic liquids. Geometrical complexity (mixing tanks, interstitial liquid in suspensions) was essential in these application, and therefore computational efficiency was crucial. Purely viscous thixotropic behaviour can be simulated with a Navier-Stokes solver that is able to handle variable viscosity, combined with a (non-diffusive) scalar transport solver for keeping track of local network integrity. The network integrity is fed back to the Navier-Stokes solver by means of a relation between network integrity and apparent viscosity. As the Navier-Stokes solver we employed a lattice-Boltzmann scheme, for solving the scalar transport equation a finite volume solver with TVD discretization. The latter for minimizing numerical diffusion. The feasibility and accuracy of the approach was assessed with a plane Poiseuille flow benchmark.

Applying this approach to laminar and transitional stirred tank flow showed the essential role of the liquid's time scale on the overall flow behaviour in the tank. Liquids with the same steady state rheology, but different time response (i.e. flow systems with different Deborah number) evolve differently towards markedly different

steady states. At  $Db = \frac{N}{k_2} = 1$  the liquid behaves almost the

same as its infinitely fast, shear thinning equivalent. At  $Db=100$  the liquid is so slow compared to mixing that the level of network development is typically uniform in the tank leading (in the case investigated here) to laminar flow. At the in-between Deborah number of 10 the flow develops in a peculiar manner, being the result of a subtle interplay between flow and liquid time scales. In this latter case the liquid is mobilized in a limited portion of the tank volume only.

Subsequently we studied drag forces in random, monosized sphere assemblies immersed in shear thinning and thixotropic liquids. As a result of the tortuous flow through the sphere assembly and its associated broad spectrum of deformation rates, shear thinning effects on drag are significant with a strong influence of the solids volume fraction (the higher, the more tortuous the flow). The effect of the solids volume fraction could be quite well captured by scaling the liquids characteristic shear rate thinning effects with the superficial velocity over the average waist of two neighbouring spheres. The effect of thixotropy is a smoothing effect on the apparent viscosity in the suspension, which in general leads to increased (by some 20%) drag.

An essential feature when studying thixotropic (and more generally non-Newtonian) flow is the rapid growth of the parameter space with increasing complexity of the liquid model. As an example: in Newtonian stirred tank flow – once the flow geometry has been defined – the only dimensionless number that matters is the Reynolds number (assuming we do not have a free liquid surface).

In this paper (with a relatively simple liquid model) we needed four dimensionless groups to pin down the flow. This makes our results less general (i.e. more specific to the model used). However, the tools developed here can be used to study specific (industrial) liquids. Furthermore, the simulations do show interesting features related to liquid mobility (in mixing tanks) and drag force behaviour (in solid-liquid suspensions).

## REFERENCES

- CHEN, S. and DOOLEN, G.D., (1998), "Lattice Boltzmann method for fluid flows", *Annu. Rev. Fluid Mech.*, **30**, 329.
- DERKSEN, J. and Van den AKKER, H.E.A., (1999), "Large-eddy simulations on the flow driven by a Rushton turbine", *AIChE J.*, **45**, 209.
- DERKSEN, J.J., (2000), "Simulation of vortex core precession in a reverse-flow cyclone", *AIChE J.*, **46**, 1317.
- DERKSEN, J.J., (2005), "Simulations of confined turbulent vortex flow", *Computers & Fluids*, **34**, 283.
- DERKSEN, J.J., (2008) "Scalar mixing by granular particles", *AIChE J.*, **54**, 1741.
- DULLAERT, K. and MEWIS, J., (2005), "Thixotropy: Build-up and breakdown curves during flow", *J. Rheol.*, **49**, 1213.
- EGGELS, J.G.M. and SOMERS, J.A., (1995), "Numerical simulation of free convective flow using the lattice-Boltzmann scheme", *Intl. J. Heat Fluid Flow*, **16**, 357.
- GOLDSTEIN, D., HANDLER, R. and SIROVICH, L., (1993), "Modeling a no-slip flow boundary with an external force field", *J. Comp. Phys.*, **105**, 354.
- FRISCH, U., HASSLACHER, B. and POMEAU, Y., (1986), "Lattice-gas automata for the Navier-Stokes Equation", *Phys. Rev. Lett.*, **56**, 1505.
- HARTMANN, H., DERKSEN, J.J., MONTAVON, C., PEARSON, J., HAMILL, I.S. and Van den AKKER, H.E.A., (2004), "Assessment of large eddy and RANS stirred tank simulations by means of LDA", *Chem. Engng. Sc.*, **59**, 2419.
- HARTMANN, H., DERKSEN, J.J. and Van den AKKER, H.E.A., (2006), "Numerical simulation of a dissolution process in a stirred tank reactor", *Chem. Engng. Sc.*, **61**, 3025.
- KANDHAI, D., DERKSEN, J.J. and Van den AKKER, H.E.A., (2003), "Interphase drag coefficients in gas-solid flows," *AIChE J.* **49**, 1060.
- MASLIYAH, J., ZHOU, Z.J., XU, Z., CZARNECKI, J. and HAMZA, H., (2004), "Understanding water-based bitumen extraction from Athabasca oil sands", *Can. J. Chem. Engng.*, **82**, 628.
- MOORE, F., (1995), "The rheology of ceramic slips and bodies", *Trans. Br. Ceramic Soc.*, **58**, 470.
- MUJUMDAR, A., BERIS, A.N. and METZNER, A.B., (2002), "Transient phenomena in thixotropic systems", *J. Non-Newtonian Fluid Mech.*, **102**, 157.
- LADD, A.J.C., (1994), "Numerical simulations of particle suspensions via a discretized Boltzmann equation. Part 2. Numerical results," *J. Fluid Mech.*, **271**, 311.
- LI, J. and KUIPERS, J.A.M., (2003), "Gas-particle interactions in dense gas-fluidized beds," *Chem. Engng. Sci.*, **58**, 711.
- SOMERS, J.A., (1993), "Direct simulation of fluid flow with cellular automata and the lattice-Boltzmann equation", *Appl. Sci. Res.*, **51**, 127.
- STOREY, B.T. and MERRILL, E.W., (1958), "The rheology of aqueous solution of amylose and amylopectine with reference to molecular configuration and intermolecular association", *J. Polym. Sci.*, **33**, 361.
- SUCCI, S., (2001), *The lattice Boltzmann equation for fluid dynamics and beyond*, Clarendon Press, Oxford.
- SUKOP, M.C. and THORNE, D.T.Jr., (2006), *Lattice Boltzmann Modeling: An Introduction for Geoscientists and Engineers*, Springer, Berlin.
- SWEBY, P.K., (1984) "High resolution schemes using flux limiters for hyperbolic conservation laws", *SIAM J. Numer. Anal.*, **21**, 995.
- Van der HOEF, M.A., BEETSTRA, R. and KUIPERS, J.A.M., (2005), "Lattice-Boltzmann simulations of low-Reynolds-number flow past mono- and bidisperse arrays of spheres: results for the permeability and drag force," *J. Fluid Mech.*, **528**, 233.
- VIKHANSKY, A., (2008), "Lattice-Boltzmann method for yield-stress liquids", *J. Non-Newtonian Fluid Mech.*, **155**, 95.
- YOSHINO, M., HOTTA, Y., HIROZANE, T. and ENDO, M., (2007), "A numerical method for incompressible non-Newtonian fluid flows based on the lattice Boltzmann method", *J. Non-Newtonian Fluid Mech.*, **147**, 69.